complexes been used as molecular probes to characterize DNA polymorphism, but they have also been central in the development of synthetic restriction enzymes.[36] Interest in the fundamental interactions between metal ions and nucleotides is enhanced by the growing body of evidence from molecular studies that such interactions may play a major role in genetic expression.

Acknowledgment. This research was supported by the National Institutes of Health in the form of a research grant to J.E.S. (GM 13,116). J.P.B. gratefully acknowledges support from the B. F. Goodrich Corp. in the form of a research fellowship.

Supplementary Material Available: Table II, listing kinetic data for the interaction of Ni(II) with NAD and NADP (5 pages). Ordering information is given on any current masthead page.

(36) Barton, J. K. *Chem. Eng. News* **1988**, *66*, 30-42.
(37) We have included the mechanism for the Ni-FAD system to provide a comparison and to minimize confusion when individual steps in the metal-mononucleotide and -dinucleotide systems, are compared. A single numbering system is used throughout.

Contribution from the NMR Section, Department of Radiology, Massachusetts General Hospital and Harvard Medical School, Boston, Massachusetts 02114

Structure-Affinity Relationships in the Binding of Unsubstituted Iron Phenolate Complexes to Human Serum Albumin. Molecular Structure of Iron(III) *N,N'*-Bis(2-hydroxybenzyl)ethylenediamine-*N,N'*-diacetate

Scott K. Larsen, Bruce G. Jenkins, Nasim G. Memon, and Randall B. Lauffer*

Received May 1, 1989

Structure-affinity relationships in the binding of iron(III) ethylene-*N,N'*-bis((2-hydroxyphenyl)glycinate) [Fe(EHPG)$^-$] diastereomers and iron(III) *N,N'*-bis(2-hydroxybenzyl)ethylenediamine-*N,N'*-diacetate [Fe(HBED)$^-$] to human serum albumin (HSA) are elucidated with equilibrium dialysis and water proton NMR relaxation studies. Fe(HBED)$^-$ and the racemic (*RR* + *SS*) isomer of Fe(EHPG)$^-$ bind to one apparent site on HSA with association constants on the order of (1.1-1.7) × 10^3 M^{-1}, whereas the meso (*RS*) isomer of Fe(EHPG)$^-$ binds only weakly. The relative affinities are apparently a function of phenolate ring orientation: the cis-equatorial phenolate coordination exhibited by *rac*-Fe(EHPG)$^-$ and Fe(HBED)$^-$ leads to a cylindrical shape that may be more complementary with a cleftlike site on the protein surface than the more distorted *meso*-Fe(EHPG)$^-$ isomer, which has one axial and one equatorial phenolate. The outer-sphere relaxivities of all three complexes increase by factors of 3-4 upon binding to the protein due to the increased rotational correlation time; this enhancement is consistent with the chelates binding on the protein surface. An X-ray structural analysis was performed on K[Fe(HBED)]·CH_3OH·$CHCl_3$, which crystallizes in the monoclinic $P2_1/a$ space group, with a = 12.589 (2) Å, b = 17.414 (2) Å, c = 12.727 (2) Å, β = 102.54°, and Z = 4.

Introduction

The characterization of noncovalent interactions between metal complexes and biological macromolecules is becoming increasingly important as new metal-containing drugs and molecular probes are being developed. For example, in vivo binding of paramagnetic complexes used as contrast-enhancing agents in ^{1}H NMR imaging can alter water relaxation properties as well as the biodistribution of the agents.[1] Secondly, the specificity of DNA-metal complex interactions, which offer new chemical and photochemical tools for molecular biology, is controlled by noncovalent binding.[2] And finally, specific monoclonal antibodies that recognize metal chelates are currently being examined for applications in radioisotope imaging and therapy.[3]

We have been interested in molecular interactions between human serum albumin (HSA) and a series of iron phenolate chelates, which are prototype liver-enhancing agents for NMR imaging.[1,4-7] These chelates include various 5-substituted derivatives of iron(III) ethylene-*N,N'*-bis((2-hydroxyphenyl)-glycinate) [Fe(EHPG)$^-$] and iron(III) *N,N'*-bis(2-hydroxybenzyl)ethylenediamine-*N,N'*-diacetate [Fe(HBED)$^-$], schematic structures for which are shown in Figure 1. Like many hydrophobic drugs and endogenous metabolites, these complexes are transported in the blood bound to HSA. Previous studies have shown that the racemic and meso isomers of Fe(5-Br-EHPG)$^-$ bind differently to HSA, with the racemic isomer having higher binding affinity and apparent localization into a specific site on the protein that also binds the heme breakdown product, bilirubin-IXα.[6] These observations raise the possibility that the three-dimensional shape of the racemic isomer more closely approximates that of bilirubin when bound to HSA. In any event, its shape is certainly important for high binding affinity.

In this work, we extend our studies to the unsubstituted derivatives of Fe(EHPG)$^-$ and Fe(HBED)$^-$. Lacking the hydrophobic bromine substituents, these derivatives possess much lower affinity for HSA; this complicates the analysis of HSA binding affinity by conventional techniques. However we are able to show by both equilibrium dialysis and water ^{1}H relaxation studies that the preferential binding of the racemic isomer holds for these chelates as well. Moreover, the relatively high binding affinity exhibited by Fe(HBED)$^-$, for which our structural analysis reveals a phenolate orientation more closely resembling the racemic isomer, affirms the importance of overall shape in the interactions between HSA and this class of rigid anionic molecules.

Experimental Section

Preparation of Complexes. Fe(EHPG)$^-$ was prepared by the addition of 1 equiv of EHPG (Sigma) and 1 equiv of NaOH to an aqueous solution of $FeCl_3$. After refluxing for 0.5-1.0 h, the solution was evaporated to dryness. The sodium salts of the meso and racemic diastereomers of Fe(EHPG)$^-$ were isolated by fractional crystallization of the residue in methanol (the meso isomer is first to crystallize) and purified

(1) Lauffer, R. B. *Chem. Rev.* **1987**, *87*, 901-927.
(2) Barton, J. K. *Science* **1986**, *233*, 727-734.
(3) Meares, C. F. *Nucl. Med. Biol.* **1986**, *13*, 319-324.
(4) Lauffer, R. B.; Greif, W. L.; Stark, D. D.; Vincent, A. C.; Wedeen, V. J.; Brady, T. J. *J. Comput. Assist. Tomogr.* **1985**, *9*, 431-438.
(5) Lauffer, R. B.; Vincent, A. C.; Padmanabhan, S.; Villringer, A.; Saini, S.; Elmaleh, D. R.; Brady, T. J. *Magn. Reson. Med.* **1987**, *4*, 582-590.
(6) (a) Lauffer, R. B.; Vincent, A. C.; Padmanabhan, S.; Meade, T. J. *J. Am. Chem. Soc.* **1987**, *109*, 2216-2218. (b) Jenkins, B. G.; Armstrong, E.; Lauffer, R. B. *Magn. Reson. Med.*, in press.
(7) Lauffer, R. B.; Betteridge, D. R.; Padmanabhan, S.; Brady, T. J. *Nucl. Med. Biol.* **1988**, *15*, 45-46.

0020-1669/90/1329-1147$02.50/0

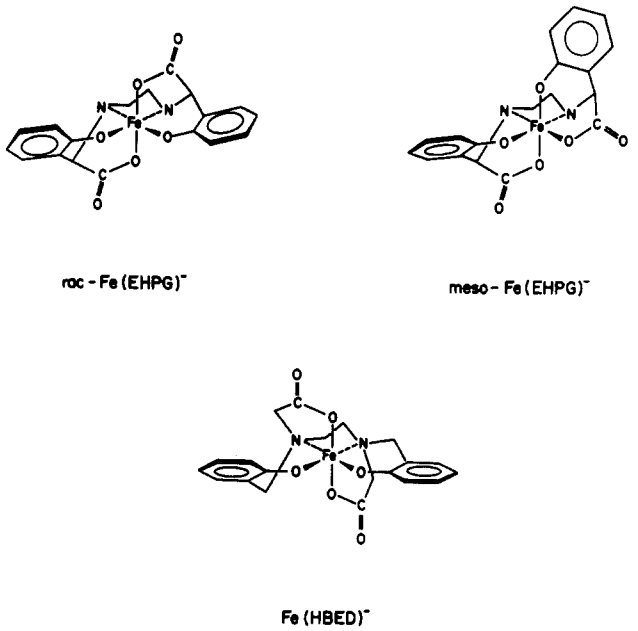

Figure 1. Schematic structures of the iron phenolate complexes.

Table I. Crystal Data and Details of the Structure Determination for $K[Fe(C_{20}H_{20}N_2O_6)]\cdot CH_3OH\cdot CHCl_3$

Crystal Data			
formula	$KFeC_{22}H_{25}N_2O_7Cl_3$	V, Å^3	2723 (1)
		Z	4
M_r	630.75	d_{calc}, g cm^{-3}	1.54
space group[a]	$P2_1/a$	d_{expt}, g cm^{-3}	1.56 (2)
cryst system	monoclinic	$F(000)$	1292
a, Å	12.589 (2)	μ, cm^{-1}	10.44
b, Å	17.414 (2)	cryst dimens, mm	0.30 × 0.30 × 0.05
c, Å	12.727 (2)		
β, deg	102.54 (1)		

Data Collection and Reduction			
diffractometer	Enraf-Nonius CAD4	scan technique	θ–2θ
data collected	$+h,+k,\pm l$	scan range (2θ), deg	45
radiation (λ, Å)	Mo Kα (0.71069)	no. of unique refl measd	6694
monochromator angle, deg	12.2	no. of obsd refl criterion	$I > 3\sigma(I)$
T, K	208	abs cor	none

Structure Determination and Refinement			
programs used	TEXSAN[b]	ratio of observns to params	8.11
scattering factors	neutral atoms[c]	max shift/error (non-H)	0.03
R_1, R_2[d]	0.060, 0.059	residual electron density, e/Å^3	0.67
weight	$4F_o^2/\sigma^2(F_o^2)$		
no. of params	331	GOF	1.34

[a] *International Tables for X-ray Crystallography*; Kynoch: Birmingham, England, 1987; Vol. 1. [b] TEXSAN-TEXRAY Structure Analysis Package, Molecular Structure Corp., 1985. [c] *International Tables for X-ray* Crystallography; Kynoch: Birmingham, England, 1974; Vol. 4, pp 71, 148. [d] The quantity minimized in the least-squares procedures is $\sum w(|F_o| - |F_c|)^2$.

by silica gel chromotography (60:40 $CHCl_3$:MeOH mixture). $K[Fe(HBED)]\cdot CH_3OH\cdot CHCl_3$ was prepared in a similar fashion from HBED (Strem Chemicals).

Crystallographic Study of Fe(HBED)$^-$. Red crystalline plates of $K[Fe(HBED)]\cdot CH_3OH\cdot CHCl_3$ grown from methanol/chloroform mixtures were found to decompose readily via solvent evaporation upon exposure to air. A suitable crystal was mounted on a glass fiber under oil, and the fiber was immediately aligned on an Enraf-Nonius CAD4 automated diffractometer under a stream of nitrogen at 208 K. Information regarding the structure determination is given in Table I. Crystal quality was examined by the peak profiles of ω scans for which half-height peak widths measured 0.25° and by the comparison of reflection intensities across the mirror plane. Three standard reflections monitored during data collection showed only statistical fluctuations in intensity.

The locations of the iron atom and several lighter atoms were obtained by direct methods using the TEXSAN package, and the positions of all other atoms were determined from the phases generated by refinement of the iron atom. Although the solution and refinement of the Fe(HBED)$^-$ anion as well as the chloroform and methanol solvates were straightforward, positional disorder problems were encountered in refinement of the potassium ions about the inversion centers $^1/_2$, 0, 0 and 0, 0, 0 in the $P2_1/a$ space group.[8a] Hydrophilic channels through the unit cell allow a disorder of electron density about these inversion centers. Within the channels, occupation of K^+ ions was based primarily on interatomic distances to well-established oxygen atoms in the lattice and secondarily on the magnitude of their respective thermal parameters. Although the K^+ ion at $^1/_2$, 0, 0 refines well anisotropically, the ion at 0, 0, 0 is less fixed and was ultimately refined as occupational fractions with free positional parameters and fixed isotropic thermal parameters.[8b] As a result of the distribution of K^+ ions, approximately 10% of the total positive charge in the unit cell (which should be 4+) was diffusely distributed about the 0, 0, 0 inversion center. This problem has been observed in a number of EHPG structures.[9,10] We note that many of the anomalous thermal parameters observed in the present structure may be due to the unresolved disorder in the potassium counterions.

Although some hydrogen atoms were located by difference maps, fixed contributions for all hydrogens were included by assuming idealized positions and a C–H bond length of 0.98 Å. The largest parameter shift

Table II. Positional parameters and B(eq) for $K[Fe(C_{20}H_{20}N_2O_6)]\cdot CH_3OH\cdot CHCl_3$

atom	x	y	z	B(eq), Å^2
Fe	0.1959 (1)	0.19736 (6)	−0.0249 (1)	2.50 (5)
K1	$^1/_2$	0	0	5.8 (2)
K2	−0.098 (2)	0.005 (1)	0.031 (2)	8.0
K3	0.086 (2)	0.003 (1)	0.056 (2)	8.0
K4	0	0	0	8.0
Cl1	0.7909 (2)	0.0081 (1)	0.3335 (2)	5.7 (1)
Cl2	0.6818 (3)	0.1465 (2)	0.3731 (2)	6.6 (2)
Cl3	0.6136 (3)	0.0016 (2)	0.4412 (2)	8.4 (2)
O1	0.0807 (5)	0.1516 (3)	−0.1254 (4)	3.7 (3)
O2	0.1822 (6)	0.1487 (3)	0.1037 (5)	5.3 (4)
O3	0.3154 (6)	0.1224 (3)	−0.0466 (5)	4.2 (3)
O4	0.4256 (5)	0.0815 (4)	−0.1479 (5)	6.0 (4)
O5	0.1111 (4)	0.2946 (3)	−0.0095 (4)	3.4 (3)
O6	0.1014 (5)	0.3998 (3)	0.0878 (4)	3.6 (3)
O10	0.3657 (5)	0.0058 (3)	0.1056 (5)	4.9 (3)
N1	0.2532 (5)	0.2497 (3)	−0.1612 (5)	2.0 (3)
N2	0.3237 (5)	0.2724 (3)	0.0694 (5)	2.2 (3)
C1	0.229 (1)	0.1614 (5)	0.2080 (7)	4.4 (5)
C2	0.177 (1)	0.1346 (5)	0.2869 (9)	5.4 (6)
C3	0.222 (1)	0.1435 (6)	0.393 (1)	6.7 (7)
C4	0.321 (1)	0.1795 (7)	0.427 (1)	6.9 (8)
C5	0.374 (1)	0.2067 (6)	0.3501 (8)	5.3 (5)
C6	0.330 (1)	0.1982 (5)	0.2397 (7)	3.9 (5)
C7	0.3921 (7)	0.2265 (4)	0.1586 (7)	3.7 (4)
C8	0.3881 (6)	0.2977 (5)	−0.0077 (7)	2.8 (4)
C9	0.3151 (7)	0.3186 (4)	−0.1149 (7)	2.9 (4)
C10	0.1561 (7)	0.2721 (5)	−0.2448 (7)	3.2 (4)
C11	0.0883 (7)	0.2052 (5)	−0.2960 (6)	2.9 (4)
C12	0.055 (1)	0.1980 (6)	−0.4055 (8)	5.7 (6)
C13	−0.011 (1)	0.1401 (7)	−0.4558 (8)	6.5 (7)
C14	−0.0446 (8)	0.0848 (6)	−0.3918 (8)	4.6 (5)
C15	−0.0121 (7)	0.0899 (5)	−0.2825 (7)	3.2 (4)
C16	0.0549 (6)	0.1492 (5)	−0.2331 (7)	2.4 (4)
C17	0.3224 (7)	0.1941 (6)	−0.2028 (7)	3.3 (4)
C18	0.3580 (8)	0.1267 (5)	−0.1271 (8)	3.7 (5)
C19	0.2714 (6)	0.3375 (4)	0.1130 (6)	2.3 (4)
C20	0.1526 (7)	0.3449 (5)	0.0590 (7)	2.5 (4)
C30	0.6678 (7)	0.0478 (5)	0.3440 (7)	4.2 (5)
C40	0.3675 (8)	−0.0071 (5)	0.214 (1)	4.9 (5)

(8) (a) The space group setting $P2_1/a$ was chosen over the customary $P2_1/c$ setting on the basis of the convention that the unit cell axis c be greater than axis a. (b) Analysis of the final positions of the potassium ions revealed octahedral coordination by six oxygen atoms in both cases. K1, located at the inversion center $^1/_2$, 0, 0, is coordinated by the carboxylate oxygens O4, O6, O4′, and O6′ and the methanol oxygens O10 and O10′ with typical bond lengths of 2.301–2.386 Å. K2, located at 0, 0, 0, is coordinated by phenolate and methanol oxygens with apparently longer bond lengths of 2.83–3.23 Å. The results for the latter may be influenced by the disorder detected for K2.

(9) Bailey, N. A.; Cummins, D.; McKenzie, E. D.; Worthington, J. M. *Inorg. Chim. Acta* **1981**, 111–120.

(10) Riley, P. E.; Pecoraro, V. L.; Carrano, C. J.; Raymond, K. N. *Inorg. Chem.* **1983**, *22*, 3096–3103.

on the final cycle of refinement occurred with a change of 0.03 relative to its estimated standard deviation. The greatest residual electron density was near K1 with a value of 0.67 e/Å^3. Final atomic coordinates are given in Table II. Tables containing anisotropic thermal parameters, calculated structure factors, and hydrogen coordinates are available as supplementary material.

Equilibrium Dialysis Studies. ^{59}Fe-labeled samples of each of the complexes were prepared by displacing the multidentate ligands with concentrated HCl, spiking the samples with 10–100-μCi $^{59}FeCl_3$, and re-forming the complex with the addition of NaOH. Due to the kinetically inert nature of the complexes, incomplete exchange was noted, even at elevated temperatures, in radio-TLC scans of samples where the ligands were not initially displaced. The labeled complexes were further purified of free iron, ligand, or salt by silica gel chromotography (60:40 $CHCl_3$:MeOH mixture) and were shown to be >95% pure by radio-TLC. (The R_f values for the complexes in this eluent were found to be 0.43, 0.35, and 0.51 for *rac*-Fe(EHPG)$^-$, *meso*-Fe(EHPG)$^-$, and Fe(HBED)$^-$, respectively.)

HSA (Sigma, crystalline) was defatted and deionized according to literature procedures.[11] H_3PO_4 replaced HCl in the procedure in order to eliminate the nonspecific displacement of the complexes by chloride ion.

Equilibrium dialysis studies were conducted at 5 °C by dialyzing 0.2- or 1.0-mL solutions of 0.3–0.5 mM HSA in 0.1 M sodium phosphate buffer, pH 7.4, against similar volumes of the labeled complexes at various concentrations (0.05–5 mM) in the same buffer. Absorption maxima and extinction coefficients for determining the concentration of the complexes were obtained from the literature.[12] The dialysis cells were rotated overnight to ensure the establishment of equilibrium. Displacement studies were performed with ibuprofen and bilirubin-IXα, both from Sigma. Stock solutions of bilirubin in 0.1 M NaOH were prepared under a red lamp and used within 10 min.

The data were plotted in the form of a Scatchard plot, r/C_{free} vs r, where r is the moles of iron complex bound per mole of HSA, and C_{free} is the free concentration of the complex. Since it appeared that the *rac*-Fe(EHPG)$^-$ and Fe(HBED)$^-$ complexes bound to a single site of modest affinity and additional weaker sites, the data were fit to the following equation:

$$r = \frac{K_1 C_{free}}{1 + K_1 C_{free}} + P C_{free} \quad (1)$$

where K_1 is the association constant (in M^{-1}) of the main site and P (also in units of M^{-1}) represents a simple partition coefficient which accounts for the high-capacity, low-affinity binding that is often present in HSA–ligand interactions.[13] The best values of K and P to fit a list of r/C_{free} values was determined by using a least-squares program that steps through values of the binding constants and minimizes the agreement factor R, defined as

$$R = \left(\frac{\sum_i (r_{calc} - r_{obs})_i^2}{\sum_i (r_{obs})_i^2} \right)^{1/2} \quad (2)$$

Proton Relaxation Enhancement (PRE) Studies. The enhancement of the water proton relaxivity of the complexes upon binding to HSA was examined by measuring longitudinal relaxation times (T_1) of solutions containing the protein and increasing concentrations of the complexes. T_1 values were measured at either 5 or 37 °C by using a 20-MHz IBM Minispec NMR spectrometer equipped with a variable-temperature probe. Eight magnetization data points were obtained with the inversion recovery method; five to seven values of T_1 were averaged for each addition of chelate.

Data for each chelate were plotted in the form of PRE_{obs} vs the molar ratio of total chelate to HSA. PRE_{obs} is defined as

$$PRE_{obs} = \frac{(1/T_1)_{obs} - (1/T_1)_{HSA}}{(1/T_1)_{free} - (1/T_1)_{H_2O}} \quad (3)$$

where $(1/T_1)_{obs}$ is the observed relaxation rate, $(1/T_1)_{HSA}$ is the relaxation rate of the HSA solution alone, $(1/T_1)_{free}$ is the relaxation rate of a buffer solution containing the same concentration of chelate and no HSA, and $(1/T_1)_{H_2O}$ is the relaxation rate of the buffer solution alone.

As described for the analysis of the equilibrium dialysis data, we elected to analyze the PRE data using a similar computational approach

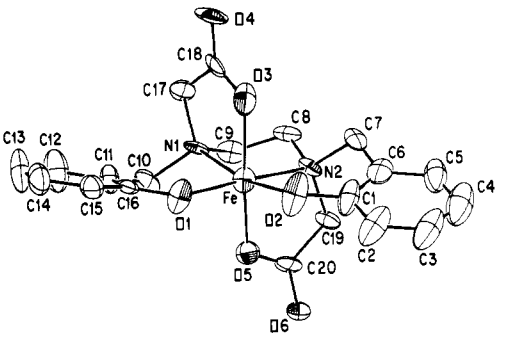

Figure 2. ORTEP drawing of the Fe(HBED)$^-$ molecular ion.

with the assumption that three forms of the chelate will exist in the HSA solution: free and bound to either a relatively specific single site or to nonspecific sites. The PRE_{obs} can then be described as a sum of mole fraction weighted PRE values:

$$PRE_{obs} = \chi_1 PRE_1 + \chi_P PRE_P + \chi_{free} PRE_{free} \quad (4)$$

where PRE_1 and PRE_P are the PRE values in the specific and nonspecific sites, respectively. The value of PRE_{free} is taken as 1.0. For fitting purposes, eq 4 can be written in terms of binding constants (as described above), PRE values, and the free and total concentrations of chelate:

$$PRE_{obs} = \frac{[HSA]_{tot}}{C_{tot}} \left(\frac{K_1 C_{free} PRE_1}{1 + K_1 C_{free}} + P C_{free} PRE_P \right) + \frac{C_{free}}{C_{tot}} \quad (5)$$

Results and Discussion

Molecular Structure of Fe(HBED)$^-$. The structural analysis of Fe(HBED)$^-$ reveals a pseudooctahedral N_2O_4 environment about the central high-spin ferric center with full hexadentate coordination by the phenolic, carboxylate, and tertiary nitrogen donors (see Figure 2). The molecule has pseudo-C_2 symmetry. As seen in the structure of *rac*-Fe(EHPG)$^-$,[9] the phenolates coordinate in a cis configuration in the equatorial plane containing the iron and nitrogen atoms; the carboxylates are trans to one another in the axial positions. The preference of six-membered chelate rings, which have larger bite angles, for the equatorial configuration has been observed previously.[14]

A more detailed comparison of Fe(HBED)$^-$ and *rac*-Fe(EHPG)$^-$ reveals that the placement of carboxylate groups on the benzyl carbons on the latter results in structural distortions in the chelate. (Quantitative comparisons are made with the Mg[Fe(EHPG)]^2·9H_2O structure in ref 9.) As can be seen in the schematic diagrams of the chelates in Figure 1, the structural requirements for the axial coordination of the EHPG carboxylates force the benzyl carbons further from the equatorial plane; this results in a twisting of the relative positions of the phenolate rings to a dihedral angle of 65.6° compared to 28.4° for Fe(HBED)$^-$. This twisting phenomenon in *rac*-Fe(EHPG)$^-$ is also accompanied by a further departure from perfect octahedral symmetry, as evidenced by bond angles about the metal center; for example, the O1–Fe–O2 bond angle increases from 101.3 to 105.5° and the N1–Fe–N2 angle decreases from 81.8 to 79.9° on going from Fe(HBED)$^-$ (Table III) to *rac*-Fe(EHPG)$^-$. The dihedral angle between the O1–Fe–O2 and N1–Fe–N2 planes, which should be zero in perfect octahedral symmetry, increases from 11.9° in Fe(HBED)$^-$ to 15.8° in *rac*-Fe(EHPG)$^-$.

Bond lengths about the metal center are also sensitive to the ligand connectivity. The more octahedral Fe(HBED)$^-$ apparently has stronger iron–phenol interactions, as evidenced by a mean iron–phenolate bond length of 1.887 (6) compared to 1.911 (3) Å for *rac*-Fe(EHPG)$^-$. The stronger interaction in Fe(HBED)$^-$ is consistent with its lower energy phenolate-to-iron(III) charge-transfer band [λ_{max} in water is at 485 nm compared to 475 nm for *rac*-Fe(EHPG)$^-$]; this relationship has been established for a series of iron(III) phenolate complexes.[15] On the other hand, the iron–tertiary nitrogen interaction in Fe(HBED)$^-$ is apparently

(11) Chen, R. F. *J. Biol. Chem.* **1967**, *242*, 173–181.
(12) (a) Patch, M. G.; Simolo, K. P.; Carrano, C. J. *Inorg. Chem.* **1983**, *22*, 2630–2634. (b) Katsuyama, T.; Kumai, T. *Bull. Chem. Soc. Jpn.* **1981**, *54*, 1544–1547.
(13) Hsia, J. C.; Er, S. S.; Tan, C. T.; Tinker, D. O. *J. Biol. Chem.* **1982**, *257*, 1724–1729.
(14) Bernauer, K. *Top. Curr. Chem.* **1976**, *65*, 1–35.
(15) Pyrz, J. W.; Roe, A. L.; Stern, L. J.; Que, L., Jr. *J. Am. Chem. Soc.* **1985**, *107*, 614–620.

Table III. Selected Bond Lengths and Bond Angles for $K[Fe(C_{20}H_{20}N_2O_6)]\cdot CH_3OH\cdot CHCl_3$

	Bond Lengths, Å		
Fe-O1	1.887 (6)	Fe-O2	1.887 (6)
Fe-O3	2.053 (7)	Fe-O5	2.031 (6)
Fe-N1	2.218 (6)	Fe-N2	2.212 (6)
O1-C16	1.339 (9)	O2-C1	1.35 (1)
O3-C18	1.26 (1)	O4-C18	1.23 (1)
O5-C20	1.26 (1)	O6-C20	1.250 (9)
N1-C17	1.47 (1)	N1-C9	1.48 (1)
N1-C10	1.49 (1)	N2-C8	1.471 (9)
N2-C19	1.476 (9)	N2-C7	1.50 (1)
C1-C2	1.39 (1)	C1-C6	1.40 (1)
C2-C3	1.36 (1)	C3-C4	1.38 (1)
C4-C5	1.39 (1)	C5-C6	1.40 (1)
C6-C7	1.51 (1)	C8-C9	1.52 (1)
C10-C11	1.51 (1)	C11-C12	1.37 (1)
C11-C16	1.39 (1)	C12-C13	1.37 (1)
C13-C14	1.39 (1)	C14-C15	1.36 (1)
C15-C16	1.39 (1)	C17-C18	1.53 (1)
C19-C20	1.51 (1)	K1-O6	2.301 (5)
K1-O10	2.378 (7)	K1-O4	2.386 (7)
K2-O1	2.98 (2)	K2-O2	3.23 (2)
Cl1-C30	1.73 (1)	Cl2-C30	1.76 (1)
Cl3-C30	1.74 (1)	O10-C40	1.40 (1)
	Bond Angles, deg		
O1-Fe-O2	101.3 (2)	O2-Fe-O5	98.3 (3)
O2-Fe-O3	92.1 (3)	O2-Fe-N2	89.4 (3)
O2-Fe-N1	166.6 (3)	O1-Fe-O5	94.2 (2)
O1-Fe-O3	96.9 (2)	O1-Fe-N2	167.7 (2)
O1-Fe-N1	88.7 (2)	O5-Fe-O3	163.0 (2)
O5-Fe-N2	78.0 (2)	O5-Fe-N1	89.8 (2)
O3-Fe-N2	88.7 (2)	O3-Fe-N1	77.6 (2)
N1-Fe-N2	81.8 (2)	O6-K1-O10	85.2 (2)
O6-K1-O4	89.3 (2)	O4-K1-O10	102.5 (2)
C16-O1-Fe	133.3 (5)	C1-O2-Fe	132.8 (6)
C18-O3-Fe	121.6 (6)	C20-O5-Fe	119.6 (5)
C17-N1-C9	111.8 (6)	C17-N1-C10	111.9 (6)
C17-N1-Fe	109.1 (5)	C9-N1-C10	110.5 (6)
C9-N1-Fe	104.9 (4)	C10-N1-Fe	108.2 (4)
C8-N2-C19	112.0 (6)	C8-N2-C7	111.0 (7)
C8-N2-Fe	105.0 (5)	C19-N2-C7	110.7 (6)
C19-N2-Fe	108.9 (4)	C7-N2-Fe	109.0 (5)
O2-C1-C2	119 (1)	O2-C1-C6	122 (1)
C1-C6-C7	121.8 (8)	N2-C7-C6	113.4 (7)
N2-C8-C9	111.1 (6)	N1-C9-C8	109.0 (6)
N1-C10-C11	113.9 (6)	C16-C11-C10	120.7 (7)
O1-C16-C11	122.4 (7)	O1-C16-C15	118.1 (8)
N1-C17-C18	113.2 (7)	O4-C18-O3	125 (1)
O4-C18-C17	119 (1)	O3-C18-C17	116.4 (8)
N2-C19-C20	111.9 (7)	O6-C20-O5	124.5 (8)
O6-C20-C19	117.0 (8)	O5-C20-C19	118.4 (8)

weaker than the iron–secondary nitrogen bond in *rac*-Fe(EHPG)$^-$ [mean Fe–N bond lengths of 2.215 (6) vs 2.166(3) Å, respectively], despite the higher basicity of the tertiary nitrogens. This has been observed in related structures.[16] In regard to the iron–carboxylate oxygen bond lengths, no significant differences between the two complexes are present.

The much higher metal–ligand stability constant for Fe(HBED)$^-$ (log K_{ML} = 39.7[17]) compared to *rac*-Fe(EHPG)$^-$ (log K_{ML} = 35.5[18]) must result largely from the more favorable octahedral configuration of the former. HBED was synthesized by Martell and co-workers precisely for this reason.[17] As mentioned above, the differences in Fe–O and Fe–N bond lengths in the two complexes are offsetting and thus do not appear to favor the HBED chelate. In addition, there are no obvious signs of strain in the bond lengths and angles for the EHPG ligand when compared to HBED.

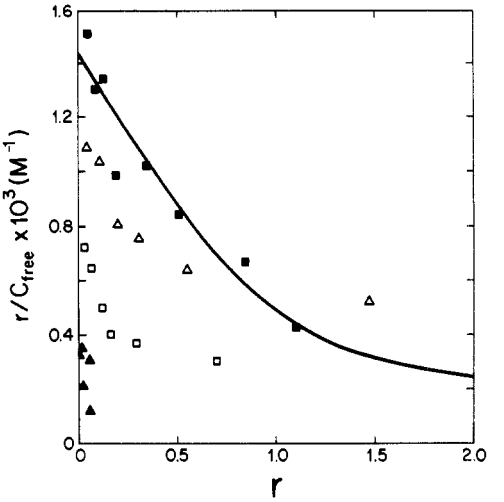

Figure 3. Scatchard plot of the binding of *rac*-Fe(EHPG)$^-$ (filled squares) and *meso*-Fe(EHPG)$^-$ (filled triangles) to HSA as measured by equilibrium dialysis. The curve through the data for the racemic isomer represents the best fit to a single site ($K = 1.3 \times 10^3$ M^{-1}) as well as to nonspecific sites. Also shown are data obtained for the racemic isomer after the addition of 1 mol of bilirubin (open squares) or ibuprofen (open triangles) per mole of HSA. r represents the molar ratio of bound chelate to HSA; C_{free} is the molar concentration of free (unbound) chelate.

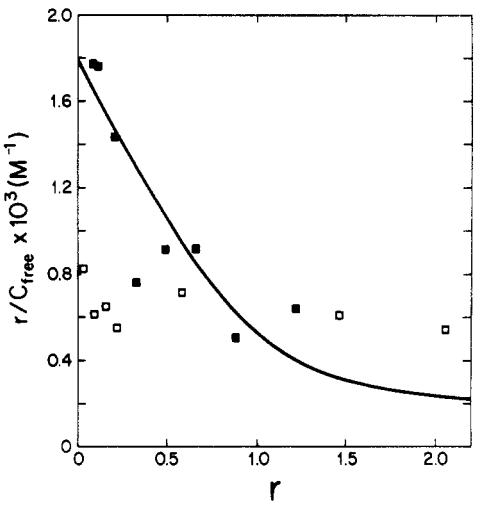

Figure 4. Scatchard plot of the binding of Fe(HBED)$^-$ to HSA as measured by equilibrium dialysis (filled squares). The curve through the data represents the best fit to a single site ($K = 1.7 \times 10^3$ M^{-1}) as well as to nonspecific sites. Also shown are data obtained after the addition of 1 mol of bilirubin (open squares) per mole of HSA.

Table IV. Binding Constants and Relaxivity Parameters for the Binding of Iron Phenolate Complexes to HSA at 5 °C

		value of fitted parameter[a]		
technique	fitted parameter	*rac*-Fe(EHPG)$^-$	Fe(HBED)$^-$	*meso*-Fe(EHPG)$^-$
equilibrium dialysis	K_1, M^{-1}	1300 ± 300	1700 ± 450	
	P, M^{-1}	140 ± 200	120 ± 250	
PRE	K_1, M^{-1}	1100 ± 200	1400 ± 300	340 ± 80
	P, M^{-1}	400 ± 100	310 ± 150	180 ± 50
	PRE_1	3.8 ± 0.2	3.0 ± 0.2	4.2 ± 0.5
	PRE_P	4.2 ± 0.4	4.2 ± 0.4	2.0 ± 0.5
	$R_{1\,free}$, mM^{-1} s^{-1} [b]	1.37	1.22	1.41

[a] Errors are 95% confidence intervals using the R factor ratio test.[22] [b] Measured in the absence of HSA.

Equilibrium Dialysis HSA-Binding Studies. Scatchard plots of the equilibrium dialysis binding data for the iron phenolate

(16) (a) Que, L., Jr.; Kolanczyk, R. C.; White, L. S. *J. Am. Chem. Soc.* **1987**, *109*, 5373–5380. (b) Chaudhuri, P. D.; Wieghardt, K.; Nuber, B.; Weiss, J. *Angew. Chem., Int. Ed. Engl.* **1985**, *24*, 778–779. (c) Lind, M. D.; Hoard, J. L.; Hamor, M. J.; Hamor, T. A. *Inorg. Chem.* **1964**, *3*, 34–43.
(17) L'Eplattenier, F.; Murase, I.; Martell, A. E. *J. Am. Chem. Soc.* **1967**, *89*, 837–843.
(18) Bannochie, C. J.; Martell, A. E. *J. Am. Chem. Soc.* **1989**, *111*, 4735–4742.

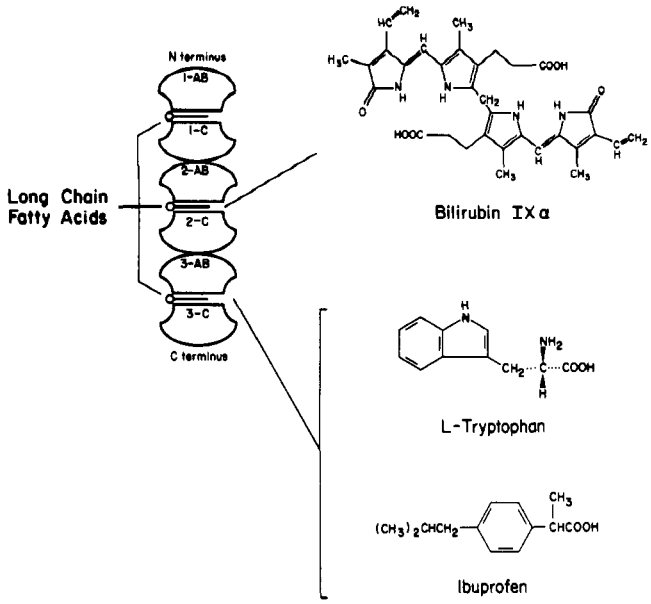

Figure 5. Schematic diagram of HSA binding sites and known ligands.

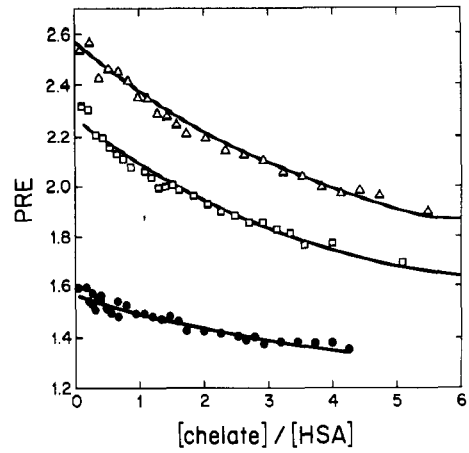

Figure 6. Proton relaxation enhancement (PRE) values as a function of added chelate for *rac*-Fe(EHPG)$^-$ (open triangles), Fe(HBED)$^-$ (open squares), and *meso*-Fe(EHPG)$^-$ (filled circles). The HSA concentration was approximately 0.6–0.8 mM. Parameters for the best-fit curves shown are given in Table IV.

complexes are shown in Figures 3 and 4. Though the data are somewhat noisy due to the low binding affinities, it is apparent that *rac*-Fe(EHPG)$^-$ and Fe(HBED)$^-$ possess moderate affinity for HSA whereas the binding of *meso*-Fe(EHPG)$^-$ is difficult to detect by this technique. In the case of the former two complexes, the data were fit to a dominant site with a binding constant K_1 of 1300 and 1700 M^{-1} for *rac*-Fe(EHPG)$^-$ and Fe(HBED)$^-$, respectively, in addition to nonspecific binding (Table IV). These values are much lower than the analogous binding constants for the 5-Br derivatives, which are in the range of 10^4–10^5 M^{-1} under similar conditions.[6]

In order to assign the binding site for *rac*-Fe(EHPG)$^-$ and Fe(HBED)$^-$ with reference to other known HSA ligands, displacement studies with bilirubin and the antiinflammatory drug ibuprofen were performed. As schematically shown in Figure 5, the most well-defined sites on HSA include that for bilirubin, that for L-tryptophan and ibuprofen (site II in the Sudlow assignment), and several for long-chain fatty acids.[19] In earlier (unpublished) work, we observed that the binding of one to two palmitate molecules per mole of HSA actually increased binding of iron phenolate chelates; this has been observed for several HSA ligands and removes the fatty acid sites as candidates for the primary binding of the chelates. Both bilirubin and ibuprofen possess high affinity for their primary sites on HSA ($K_1 \approx 10^8$ and 10^6 M^{-1}, respectively) and therefore would be expected to displace the weakly bound iron phenolate chelates when present in a 1:1 ligand:HSA ratio. In the case of *rac*-Fe(EHPG)$^-$, the addition of ibuprofen appears to reduce the binding somewhat but the overall curvature of the Scatchard plot remains roughly the same (Figure 3). Bilirubin, on the other hand, causes much greater displacement of *rac*-Fe(EHPG)$^-$, and the steep portion of the curve at low r values is likely to merely represent residual binding to a small fraction of the high-affinity sites not occupied by bilirubin. Similarly, the addition of bilirubin to Fe(HBED)$^-$ leads to a large degree of displacement and a change in the appearance of the Scatchard plot (Figure 4). These results, though not definitive assignments, are indicative of the bilirubin site as a possible primary site for binding of the iron complexes. This agrees with previous studies on the 5-Br analogues.[6]

Water Proton Relaxation Enhancement (PRE) Studies. The measurement of water ^1H relaxation times in the presence of a biological macromolecule and varying concentrations of a paramagnetic species can yield information about the number of binding sites and binding constants under favorable conditions. The increase in the rotational correlation time of the paramagnetic species upon binding leads to an increase in the efficiency of the dipolar electron–proton relaxation process. This technique, known as PRE, has been utilized extensively in the analysis of metal ion binding sites.[20,21] In the case of prototype NMR contrast agents, such as the chelates in this work, binding to proteins, PRE studies are crucial to understanding in vivo relaxation behavior.[1]

The addition of HSA to an iron chelate solution increases the relaxivity of the chelate roughly 2-fold, depending on the chelate, due to noncovalent binding. If the chelate is added in excess, the enhancement in relaxivity, or PRE, decreases as the free fraction increases. PRE plots for the three iron chelates are shown in Figure 6. It is apparent that the average PRE values are higher for the chelates with moderate binding affinities than for the weaker binding *meso*-Fe(EHPG)$^-$. The higher PRE values for the former complexes are most likely due to a higher mole fraction bound to HSA rather than any large differences in relaxivities of the bound chelates.

The PRE plots were fit to eq 5, providing corroborative estimates of the binding constants as well as estimates of the relaxivity of each chelate when bound to the protein. A single "high-affinity" site was assumed with nonspecific binding taken into account as described in the Experimental Section. (Use of fewer parameters in the fits, such as the case where nonspecific binding is omitted from the model, led to unacceptable fits.) As shown in Table IV, the resulting binding constants for *rac*-Fe(EHPG)$^-$ and Fe(HBED)$^-$ are similar to those found in the dialysis studies within the errors of the techniques. The fitted PRE values indicate that the relaxivities of the chelates increase by 3- to 4-fold upon binding.

The most significant result of the PRE studies is the ability to observe binding of the very weakly bound *meso*-Fe(EHPG)$^-$ complex, as indicated in the curvature of its PRE plot. Fitting these data to the model described above reveals a binding constant of approximately 300 M^{-1}. It is likely that the dialysis technique could not detect this low binding affinity since the difference in the concentration of the chelate on either side of the dialysis membrane would be quite small.

Conclusions

Noncovalent binding of iron phenolate complexes by HSA is influenced by the relative orientation of coordinated phenolate rings. A structural analysis of Fe(HBED)$^-$ confirms the expected cis-equatorial arrangement of the two phenolates. This complex and the racemic isomer of Fe(EHPG)$^-$, which possesses a similar phenolate orientation, bind to HSA at a single site with moderate

(19) Peters, T., Jr. *Adv. Protein Chem.* **1985**, *37*, 161–245.

(20) Dwek, R. A. *Nuclear Magnetic Resonance in Biochemistry, Applications to Enzyme Systems*; Clarendon: Oxford, U.K., 1973; Chapters 9–11.

(21) Mildvan, A. S. *Annu. Rev. Biochem.* **1974**, *43*, 357.

(22) Hamilton, W. C. *Acta Crystallogr.* **1965**, *18*, 502–510.

affinity. In contrast, *meso*-Fe(EHPG)$^-$, which has one equatorial and one axial phenolate, has much lower affinity for HSA. We suggest that, in the case of these unsubstituted derivatives with relatively low binding affinity, the overall shape of the complexes is as important as various individual contributions to the binding free energy (hydrogen bonds, van der Waals interactions, etc.). Thus, while the structures of Fe(HBED)$^-$ and *rac*-Fe(EHPG)$^-$ are quite different in some respects (e.g., the twist of the phenolate rings, the placement of carboxylate groups, and the presence of secondary nitrogens), the extended, cylindrical shape of the molecules apparently leads to similar binding activity, perhaps at a cleftlike site on the protein surface. Our studies indicate that the high-affinity bilirubin site on HSA is a likely candidate.

The binding of the chelates to HSA increases their relaxivity substantially. These coordinatively saturated complexes most likely relax water protons via transient hydrogen bonds from solvation waters.[1,6b] The observed enhancement in outer-sphere (or second-coordination-sphere) relaxivity is consistent with the binding of the chelates on the surface of HSA wherein a portion of the solvation layer of the chelate would be expected to persist.

Acknowledgment. This work was supported by PHS Grant Nos. GM37777, awarded by the National Institute of General Medical Sciences, and CA42430, awarded by the National Cancer Institute. We thank Dr. William M. Davis and the X-ray diffraction facility at the Massachusetts Institute of Technology Department of Chemistry for cooperation in this project.

Supplementary Material Available: Listings of calculated coordinates and B(eq) parameters of hydrogen atoms (Table V) and anisotropic thermal parameters for all non-hydrogen atoms (Table VI) (4 pages); a listing of final observed and calculated structure factors (Table VII) (39 pages). Ordering information is given on any current masthead page.

Contribution from the Laboratoire de Cristallographie et de Physique Cristalline (URA 144, CNRS), Université de Bordeaux I, 33405 Talence, France, and Laboratoire de Chimie Inorganique (URA 420, CNRS), Université de Paris-Sud, 91405 Orsay, France

Structural Changes Associated with the Spin Transition in $Fe(phen)_2(NCS)_2$: A Single-Crystal X-ray Investigation

Bernard Gallois,*[1a] José-Antonio Real,[1b,c] Christian Hauw,[1a] and Jacqueline Zarembowitch*[1b]

Received May 24, 1989

The crystal structure of $Fe(phen)_2(NCS)_2$ (phen = 1,10-phenanthroline) was determined by X-ray diffraction at ≈293 and ≈130 K, in order to detect the structural changes associated with the singlet ↔ quintet spin transition. The space group is *Pbcn* with $Z = 4$ at both temperatures. Lattice constants are as follows: $a = 13.1612$ (18), $b = 10.1633$ (11), and $c = 17.4806$ (19) Å at ≈293 K and $a = 12.7699$ (21), $b = 10.0904$ (25), and $c = 17.2218$ (30) Å at ≈130 K. The data were refined (167 parameters) to $R = 3.4\%$ (4.1%) at ≈293 K (≈130 K) for 1050 (1115) observed independent reflections ($F_o^2 > 2\sigma(F_o)^2$). In disagreement with most of the predictions, the transition is found to be accompanied neither by a change in the crystal symmetry nor by an order–disorder transition involving $(NCS)^-$ groups. Only a large reorganization of the iron(II) environment is detected. The main structural modifications, when passing from the high- to the low-spin form, consist of an important shortening of the Fe–N(phen) and Fe–N(CS) distances (by 0.20 (mean value) and 0.10 Å, respectively) and a noticeable variation of the N–Fe–N angles, leading to a more regular shape of the [Fe–N_6] octahedron. The temperature dependence of $\chi_m T$ (χ_m = molar magnetic susceptibility), determined on a polycrystalline sample of $Fe(phen)_2(NCS)_2$, shows the existence of a sharp transition centered at $T_c \approx 176.5$ K. The higher and lower limits of $\chi_m T$ (3.41 and 0.58 $cm^3 \cdot mol^{-1} \cdot K$) indicate that the compound is in the high-spin state at room temperature, whereas ≈17% of the high-spin isomer is retained in the low-spin form at low temperature. On account of this magnetic behavior and of the crystallographic data, the compound is assumed to be in the crystalline form "II", by analogy with $Fe(bpy)_2(NCS)_2$ (bpy = 2,2′-bipyridine).

Introduction

The compound *cis*-bis(thiocyanato)bis(1,10-phenanthroline)-iron(II), $Fe(phen)_2(NCS)_2$, has been known since the 1960s[2-5] to exhibit a discontinuous $S = 2 \leftrightarrow S = 0$ spin crossover in the solid state, at a critical temperature T_c close to 176 K.

This complex is one of the spin-crossover systems that have been most investigated.[6] Various techniques were used to study its transition: magnetic susceptibility measurements,[2,4,5,7-10] Mössbauer,[4,5,8,9,11,12] infrared,[3,5,12-16] and UV–visible[5] spectrometries, calorimetric measurements,[9,15,17] X-ray powder diffraction[2,4,5,9] and absorption (EXAFS, XANES, edge),[18] NMR spectrometry[11,19] and XPS.[20,21] In all the above-mentioned studies, the spin transition of $Fe(phen)_2(NCS)_2$ was thermally driven. However, this transition has also been induced by pressure,[22-25] by both pressure and temperature,[24-26] and by light irradiation (the phenomenon being called "light-induced excited spin state trapping" or LIESST).[16,27] On the other hand, among the additional investigations related to $Fe(phen)_2(NCS)_2$, let us point out the following: the influence of a magnetic field on the critical temperature value,[28] the effect of metal dilution on the transition

(1) (a) Université de Bordeaux I. (b) Université de Paris-Sud. (c) Permanent address: Departamento de Quimica Inorganica, Facultad de Farmacia, Universidad de Valencia, Valencia, Spain.
(2) Baker, W. A.; Bobonich, H. M. *Inorg. Chem.* **1964**, *3*, 1184.
(3) Baker, W. A.; Long, G. J. *Chem. Commun.* **1965**, *15*, 368.
(4) König, E.; Madeja, K. *Chem. Commun.* **1966**, *3*, 61.
(5) König, E.; Madeja, K. *Inorg. Chem.* **1967**, *6*, 48.
(6) Gütlich, P. *Struct. Bonding (Berlin)* **1981**, *44*, 83.
(7) Casey, A. T.; Isaac, F. *Aust. J. Chem.* **1967**, *20*, 2765.
(8) Ganguli, P.; Gütlich, P. *J. Phys.* **1980**, *41*, C1-313.
(9) Ganguli, P.; Gütlich, P.; Müller, E. W.; Irler, W. *J. Chem. Soc., Dalton Trans.* **1981**, 441.
(10) Müller, E. W.; Spiering, H.; Gütlich, P. *Chem. Phys. Lett.* **1982**, *93*, 567.
(11) Dézsi, I.; Molnar, B.; Tarnoczi, T.; Tompa, K. *J. Inorg. Nucl. Chem.* **1967**, *29*, 2486.
(12) Savage, S.; Jia-Long, Z.; Maddock, A. G. *J. Chem. Soc., Dalton Trans.* **1985**, 991.
(13) König, E.; Madeja, K. *Spectrochim. Acta* **1967**, *23A*, 45.
(14) (a) Takemoto, J. H.; Hutchinson, B. *Inorg. Nucl. Chem. Lett.* **1972**, *8*, 769. (b) *Inorg. Chem.* **1973**, *12*, 705.
(15) Sorai, M.; Seki, S. *J. Phys. Chem. Solids* **1974**, *35*, 555.
(16) Herber, R.; Casson, L. M. *Inorg. Chem.* **1986**, *25*, 847.
(17) Sorai, M.; Seki, S. *J. Phys. Soc. Jpn.* **1972**, *33*, 575.
(18) Cartier, C.; Thuéry, P.; Verdaguer, M.; Zarembowitch, J.; Michalowicz, A. *J. Phys.* **1986**, *47*, C8-563.
(19) Rao, P. S.; Ganguli, P.; McGarvey, B. R. *Inorg. Chem.* **1981**, *20*, 3682.
(20) Vasudevan, S.; Vasan, H. N.; Rao, C. N. R. *Chem. Phys. Lett.* **1979**, *65*, 444.
(21) Burger, K.; Furlani, C.; Mattogno, G. *J. Electron Spectrosc. Relat. Phenom.* **1980**, *21*, 249.
(22) Fischer, D. C.; Drickamer, H. G. *J. Chem. Phys.* **1971**, *54*, 4825.
(23) Ferraro, J. R.; Takemoto, J. *Appl. Spectrosc.* **1974**, *28*, 66.
(24) Adams, D. M.; Long, G. J.; Williams, A. D. *Inorg. Chem.* **1982**, *21*, 1049.
(25) Pebler, J. *Inorg. Chem.* **1983**, *22*, 4125.
(26) Usha, S.; Srinivasan, R.; Rao, C. N. R. *Chem. Phys.* **1985**, *100*, 447.
(27) Decurtins, S.; Gütlich, P.; Köhler, C. P.; Spiering, H. *J. Chem. Soc., Chem. Commun.* **1985**, 430.

0020-1669/90/1329-1152$02.50/0